Electron scattering from silicon

Viktor Gedeon, Sergej Gedeon, Vladimir Lazur, and Elizabeth Nagy
Department of Theoretical Physics, Uzhgorod State University, Uzhgorod, UA-88000, Ukraine

Oleg Zatsarinny* and Klaus Bartschat
Department of Physics and Astronomy, Drake University, Des Moines, Iowa 50311, USA
(Received 23 January 2012; published 21 February 2012)

The B-spline R-matrix method is used to study electron collisions with neutral silicon over an energy range from threshold to 100 eV. The multiconfiguration Hartree-Fock method with nonorthogonal orbitals is employed for an accurate representation of the target wave functions. The present close-coupling expansion includes 34 bound states of neutral silicon derived from the [Ne]$3s^2\,3p^2$, $3s3p^3$, $3s^2\,3p4s$, $3s^2\,3p5s$, $3s^2\,3p4p$, $3s^2\,3p5p$, $3s^2\,3p3d$, and $3s^2\,3p4d$ configurations, plus seven pseudostates to fully account for the dipole polarizability of the ground state and the lowest three excited states of atomic silicon. Cross sections are presented for important transitions from the $3s^2\,3p^2\,{}^3P$ ground state and the metastable $3s^2\,3p^2\,{}^1D$ and $3s^2\,3p^2\,{}^1S$ states. Both correlation and polarization effects are found to be important for accurate calculations of the cross sections. The sensitivity of the results was checked by comparing data obtained in different approximations. The current predictions represent an extensive set of electron scattering data for neutral silicon.

DOI: 10.1103/PhysRevA.85.022711 PACS number(s): 34.80.Bm

I. INTRODUCTION

Atomic silicon is among the high-abundant elements in the universe, and hence accurate atomic data for elastic scattering and electron-impact excitation for this target are important in the modeling of various astrophysical plasmas. In particular, silicon contributes significantly to the solar and stellar opacities in the ultraviolet regime. Also, silicon composite materials and its halocompounds are used in various plasma devices. Recently, silicon became widely used in nanotechnology [1–3]. It forms a nearly perfect inert surface on which to deposit biomolecules, and it is also relevant to simulations of radiation detector responses.

A detailed knowledge of different silicon properties is thus required, including accurate cross-section data for electron scattering. Nevertheless, electron collision cross sections for neutral silicon are almost absent in the literature. The difficulties in obtaining sufficient quantities of atomic silicon in the gas phase in a well-defined initial state explain the lack of cross-section measurements to date. This lack of experimental data, in turn, did not motivate sophisticated theoretical investigations, and the rare theoretical studies were carried out about 35 years ago [4]. Those authors employed simple structure and collisions models, and they were only concerned with elastic scattering from the ground state and a few transitions among the lowest excited states.

The purpose of the present paper is to provide an extensive data set of cross sections for elastic scattering from and electron-impact excitation of neutral silicon. The calculations were carried out with our highly sophisticated B-spline R-matrix (close-coupling) (BSR) code [5]. The distinct feature of the approach is its ability to employ term-dependent nonorthogonal orbitals in the description of the target states. This allows us to optimize individual atomic wave functions independently and thereby generate a much more accurate description of the target states than what is usually possible when orthogonality restrictions are imposed. Over the past decade, the BSR code (along with its fully relativistic extension, DBSR [6]) has been successfully applied to a number of targets [7], and in many cases the cross sections are more accurate than those obtained using the standard R-matrix technique. Note that the BSR suite of programs forms a general code for many-electron targets, and its advantages are particularly seen in cases of electron scattering from systems with complex configurational structure, including multiple open shells. Examples include electron scattering from the open-shell atoms O [8], S [9] and C [10], of which the latter has a similar electronic valence structure to the atomic silicon that we are interested in here.

This paper is organized as follows: After discussing the description of the target structure, we summarize the most important aspects of the collision calculations. This is followed by a presentation of the cross sections for the most important transitions, starting with elastic scattering from Si in its ground state and the lowest two excited states. Due to the lack of experimental results available for comparison, we present two sets of calculations, with 34 and 41 target states, respectively, included in the close-coupling expansion. The first model only contains physical bound states, while the second one also includes polarized pseudostates. Comparison of the results from these two calculations provides some indication about the sensitivity of the predicted cross sections on the details of the model.

II. COMPUTATIONAL DETAILS

A. Structure calculations

Neutral silicon can be considered a strongly correlated four-electron system in the $1s^2\,2s^2\,2p^6$ core potential. This makes it very difficult to obtain accurate wave functions by standard Hartree-Fock (HF) or multiconfiguration Hartree-Fock (MCHF) methods. As shown in recent large-scale MCHF

*oleg.zatsarinny@drake.edu

calculations of oscillator strengths in Si [11], well-converged results were only achieved with very extensive expansions containing up to 20 000 configurations. In the present calculations of the Si target states, we tried to account for the principal correlation effects, while bearing in mind that the final multiconfiguration expansions still need to be dealt with in the subsequent collision calculation with one more electron to be coupled in. Since relativistic effects are relatively small in silicon, the target states for the collision calculations were generated by the B-spline box-based close-coupling method [12] in the nonrelativistic LS-coupling approximation.

Specifically, the structure of the multichannel target expansion was chosen as

$$\begin{aligned}\Phi(3s^2\,3pnl, LS) &= \sum_{nl}\{\phi(3s^2\,3p)P(nl)\}^{LS} + \sum_{nl}\{\phi(3s3p^2)P(nl)\}^{LS} \\ &+ \sum_{nl}\{\phi(3s^2\,3d)P(nl)\}^{LS} + \sum_{nl}\{\phi(3s^2 4s)P(nl)\}^{LS} \\ &+ a_{LS}\varphi(3s^2\,3p^2)^{LS} + b_{LS}\varphi(3s3p^3)^{LS}. \qquad (1)\end{aligned}$$

Here $P(nl)$ denotes the wave function of the outer valence electron, while the ϕ and φ functions stand for the configuration interaction (CI) expansions of the corresponding ionic and specific atomic states, respectively. These expansions were generated in separate MCHF calculations for each state using the MCHF program [13]. The expansion (1) can be considered a model for the entire $3s^2\,3pnl$ Rydberg series of bound states in Si, perturbed by the $3s^2\,3p^2$ and $3s3p^3$ states for particular LS terms. The remaining parts in the above expansion describe the main dipole transitions $3s$–$3p$, $3p$–$3d$, and $3p$–$4s$ in the ionic states, thereby including the core-valence (long-range) correlation for the outer electrons. Inner-core (short-range) correlation is included through the CI expansion of the ionic states. These expansions include all single, double, and triple excitations from the $3s$ and $3p$ orbitals to the $4l$ and $5l$ ($l = 0$–4) correlated orbitals, which were generated separately for each state. To keep the final expansions for the atomic states to a reasonable size, all ionic contributions with expansion coefficients of magnitude less than 0.01 were neglected.

The unknown functions $P(nl)$ for the outer valence electron were expanded in a B-spline basis, and the corresponding equations were solved subject to the condition that the wave functions vanish at the boundary. The B-spline coefficients for the valence orbitals $P(nl)$, along with the coefficients a_{LS} and b_{LS} for the perturbers, were obtained by diagonalizing the atomic Hamiltonian. The above scheme yields a set of term-dependent one-electron orbitals for each valence orbital, also accounting for important interactions between the $3s^2\,3pnl$ Rydberg series and the $3s3p^3$ perturbers.

Since the B-spline bound-state close-coupling calculations generate different nonorthogonal sets of orbitals for each atomic state, their subsequent use is somewhat complicated. On the other hand, our configuration expansions for the atomic target states contained at most 200 configurations for each state and hence could be used in the collision calculations with moderate computational resources.

Table I compares the calculated spectrum of silicon with the experimental values [14] for various multiplets. The overall agreement between experiment and theory is very satisfactory, with the deviation in the energy splitting being less than 0.02 eV for most states. The maximum deviation between the present results and experiment is 0.08 eV for the $3s^2\,3p^2\,{}^1S$ state.

TABLE I. Binding energies (in eV) for the spectroscopic and pseudo (ps) target states.

	State	Term	Present	NIST [14]	Diff.
1	$3p^2$	^3P	−8.124	−8.145	0.021
2	$3p^2$	^1D	−7.326	−7.383	0.057
3	$3p^2$	^1S	−6.175	−6.255	0.080
4	$3s3p^3$	$^5S^o$	−4.093	−4.032	−0.061
5	$3p4s$	$^3P^o$	−3.180	−3.222	0.042
6	$3p4s$	$^1P^o$	−3.043	−3.082	0.039
7	$3s3p^3$	$^3D^o$	−2.529	−2.547	0.018
8	$3p4p$	^1P	−2.294	−2.302	0.008
9	$3p3d$	$^1D^o$	−2.281	−2.293	0.012
10	$3p4p$	^3D	−2.184	−2.193	0.009
11	$3p4p$	^3P	−2.057	−2.073	0.016
12	$3p4p$	^3S	−2.039	−2.039	0.000
13	$3p3d$	$^3F^o$	−1.961	−1.969	0.008
14	$3p4p$	^1D	−1.917	−1.941	0.024
15	$3p3d$	$^3P^o$	−1.886	−1.899	0.013
16	$3p4p$	^1S	−1.748	−1.765	0.017
17	$3p3d$	$^1F^o$	−1.540	−1.548	0.008
18	$3p3d$	$^1P^o$	−1.525	−1.545	0.020
19	$3p3d$	$^3D^o$	−1.434	−1.441	0.007
20	$3p5s$	$^3P^o$	−1.409	−1.416	0.007
21	$3p5s$	$^1P^o$	−1.360	−1.361	0.001
22	$3p4d$	$^1D^o$	−1.154	−1.158	0.004
23	$3p4d$	$^3P^o$	−1.146	−1.134	−0.012
24	$3p5p$	^1P	−1.122	−1.124	0.002
25	$3p5p$	^3D	−1.089	−1.085	−0.004
26	$3p5p$	^3P	−1.048	−1.047	−0.001
27	$3p4d$	$^3F^o$	−1.040	−1.036	−0.004
28	$3p5p$	^3S	−1.043	−1.030	−0.013
29	$3p5p$	^1D	−0.998	−0.998	−0.000
30	$3p5p$	^1S	−0.936	−0.934	−0.002
31	$3p4d$	$^1P^o$	−0.862	−0.874	0.012
32	$3p4d$	$^1F^o$	−0.862	−0.862	0.000
33	$3p4d$	$^3D^o$	−0.843	−0.839	−0.004
34	ps1	$^3P^o$	0.876		
35	ps2	$^3D^o$	1.189		
36	ps3	$^1F^o$	1.360		
37	$3s3p^3$	$^3S^o$	1.781	1.713	0.068
38	ps4	$^1P^o$	2.186		
39	ps5	$^1D^o$	2.221		
40	ps6	$^3S^o$	3.837		
41	ps7	^5P	4.143		

The quality of our target description can be further assessed by comparing the results for the oscillator strengths of various transitions with experimental data and other theoretical predictions. Such a comparison of our results is given in Table II with the recent large-scale MCHF calculations of Fischer [11] and the experimental data of O'Brian and Lawler. [15]. The experimental gf values for the fine-structure transitions were converted to the multiplet LS values by combining them with the appropriate weights. In most cases,

TABLE II. Comparison of weighted oscillator strengths in Si.

Lower level	Upper level	Present	MCHF [11]	Expt. [15]
$3s^2\,3p^2\,{}^3P$	$3s^2\,3p4s\,{}^3P^o$	1.907	1.908	1.893 ± 0.098
	$3s^2\,3p3d\,{}^3P^o$	0.404	0.378	0.461 ± 0.024
	$3s3p^3\,{}^3D^o$	0.471	0.394	0.501 ± 0.026
	$3s^2\,3p3d\,{}^3D^o$	1.885	2.165	
$3s^2\,3p^2\,{}^1D$	$3s^2\,3p3d\,{}^1F^o$	1.488	1.539	1.409 ± 0.073
	$3s^2\,3p4s\,{}^1P^o$	0.878	0.873	0.811 ± 0.042
	$3s^2\,3p3d\,{}^1D^o$	0.193	0.182	0.197 ± 0.010
	$3s^2\,3p3d\,{}^1P^o$	0.011	0.016	0.014 ± 0.001
$3s^2\,3p^2\,{}^1S$	$3s^2\,3p4s\,{}^1P^o$	0.103	0.097	0.091 ± 0.005
	$3s^2\,3p3d\,{}^1P^o$	0.323	0.345	0.330 ± 0.017

we see good agreement with the experimental data, although a few predictions fall outside of the experimental error bars. Overall, there is close agreement with the MCHF results [11]. The remaining discrepancies are generally due to the much smaller target expansions used in the present calculations. Accurate oscillator strengths are very important to obtain reliable absolute values for the excitation cross sections, especially for optically allowed transitions at high electron energies.

B. Polarized pseudostates

For elastic scattering at small energies, it is very important to include the polarization of the target ground state to full extent. The polarizabilities of the Si states are relatively large (see below). Furthermore, typically more than 50% of the total polarizability originates from excitation to the target continuum. This may lead to a slow convergence of the close-coupling expansion, which needs to contain a large number of pseudostates to mimic the coupling to the ionization channels. Computationally this means very extensive calculations.

A much more effective way to incorporate the target polarization is the use of so-called polarized pseudostates. They were considered in scattering problems, for example, by Burke and Mitchell [16]. In the simplest case of an atomic S state, the appropriate polarized pseudostate ψ_p can be defined by the requirement that the static electric dipole polarizability of the atomic state ψ_0 be expressed by a single term according to

$$\alpha = 2\frac{|\langle\psi_p|D^{(1)}|\psi_0\rangle|^2}{E_p - E_0}, \tag{2}$$

where $D^{(1)}$ is the electric dipole operator while E_0 and E_p are the energies of the ground state and the polarized pseudostate, respectively. As shown by Burke and Mitchell [16], ψ_p is a normalized solution of the equation

$$(H - E_0)\psi_p = D^{(1)}\psi_0, \tag{3}$$

with its energy given by

$$E_p = \langle\psi_p|H|\psi_p\rangle. \tag{4}$$

In the more general case of a state with nonzero orbital angular momentum, pseudostates for each optically allowed transition should be determined and their contributions to the dipole polarizability need to be added up (see Table III). As recently demonstrated for electron scattering from Kr [17], polarized pseudostates allow for a very accurate description of low-energy elastic scattering, based on first principles without the use of semiempirical polarization potentials.

TABLE III. Polarizabilities (in atomic units) of the lowest four target states of Si.

State	Final symmetry	Contribution to α	Other calculations
$3s^2\,3p^2\,{}^3P$	${}^3S^o$	2.84	
	${}^3P^o$	15.20	
	${}^3D^o$	19.41	
	sum	37.45	37.40 [18]
			37.17 [19]
			37.31 [20]
$3s^2\,3p^2\,{}^1D$	${}^1F^o$	11.57	
	${}^1P^o$	10.23	
	${}^1D^o$	19.60	
	sum	41.30	
$3s^2\,3p^2\,{}^1S$	${}^1P^o$	50.08	
$3s3p^3\,{}^5S^o$	${}^5P$	33.00	

Polarized pseudostates in the present calculations were obtained for several target states with the same expansion (1) as for the spectroscopic bound states. To avoid double counting, a few additional orthogonality restrictions were imposed on the bound states included. Specifically, we accounted for the polarization of the four lowest bound states. The energies of the respective polarized pseudostates are given in Table I, while the corresponding polarizabilities are listed in Table III. The total static polarizability of the ground state is in close agreement with that predicted by other recent calculations. The pseudostates also represent some effects of very important excitation channels to the higher-lying core-excited states $3s3p^3\,{}^1P$, ${}^3P$, and ${}^1D$, which are not included explicitly in the close-coupling expansion. These $3s3p^3$ states are autoionizing states that interact very strongly with the adjoint continuum. Note that a direct calculation of these states with standard atomic-structure programs is very difficult.

C. Collision calculations

The close-coupling expansion in the present work includes the 34 spectroscopic states of neutral silicon plus 7 polarized pseudostates listed in Table I. The corresponding close-coupling equations were solved with the R-matrix method by employing the BSR complex [5]. The distinctive feature of the method is the use of B splines as a universal basis to represent the scattering orbitals in the inner region of $r \leqslant a$. Hence, the R-matrix expansion in this region takes the form

$$\begin{aligned}\Psi_k(x_1,\ldots,x_{N+1}) &= \mathcal{A}\sum_{ij}\bar{\Phi}_i(x_1,\ldots,x_N;\hat{\mathbf{r}}_{N+1}\sigma_{N+1})\,r_{N+1}^{-1}\,B_j(r_{N+1})\,a_{ijk} \\ &\quad + \sum_i \chi_i(x_1,\ldots,x_{N+1})\,b_{ik}.\end{aligned} \tag{5}$$

Here the $\bar{\Phi}_i$ denote the channel functions constructed from the N-electron target states, while the splines $B_j(r)$ represent

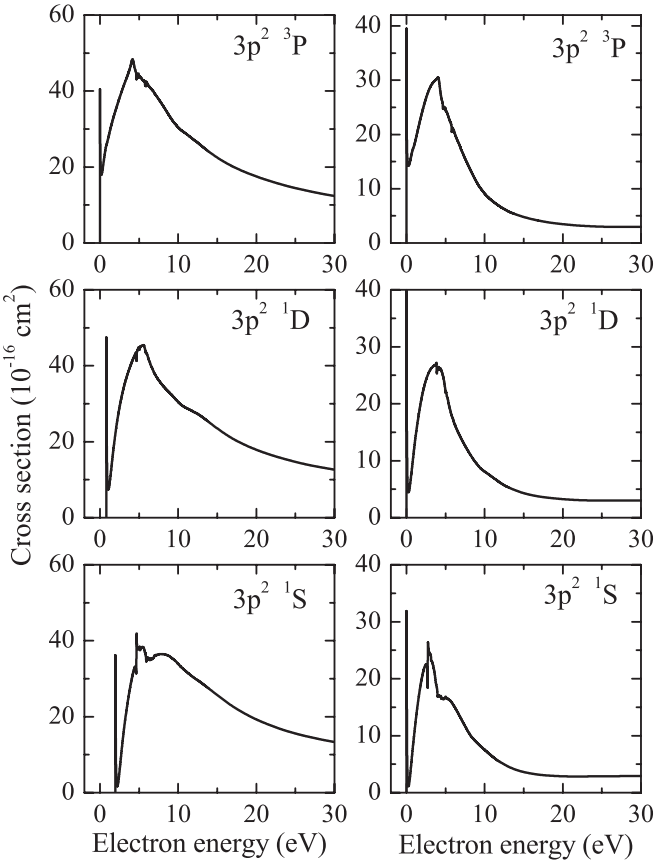

FIG. 1. Elastic (left panels) and momentum transfer (right panels) cross sections for electron scattering from the three states with the ground-state configuration $3s^2\,3p^2$.

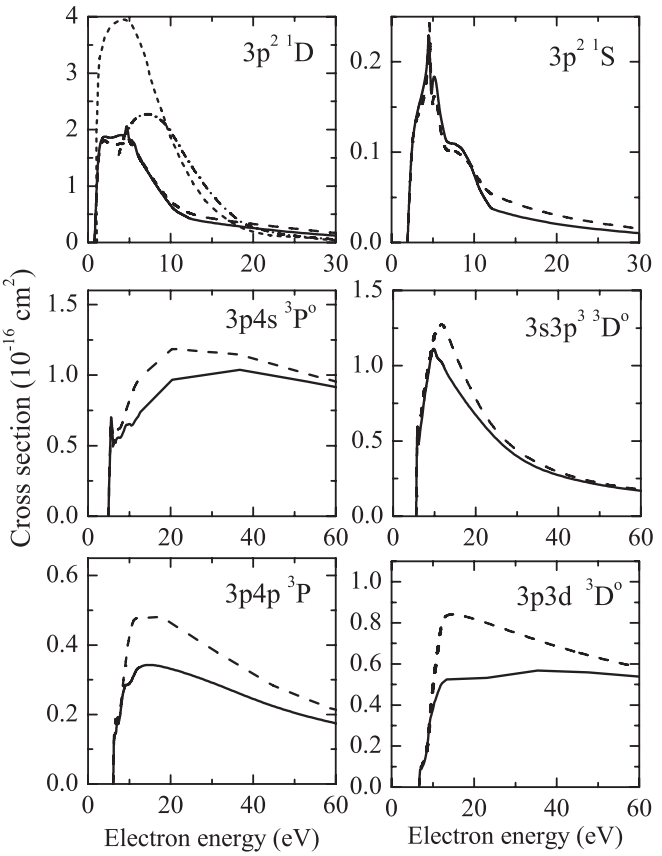

FIG. 2. Cross sections as a function of collision energy for the most important transitions from the $3s^2\,3p^2\,^3P$ ground state (solid lines), compared to results from calculations without pseudostates (long-dashed lines). Also shown are distorted-wave calculations [4] for the $^3P \rightarrow {}^1S$ transition: adiabatic-exchange method (short-dashed line), Hartree-Fock approximation (dash-dotted line).

the continuum orbitals. The χ_i are additional $(N+1)$-electron bound states. In standard R-matrix calculations [21], the latter are included one configuration at a time to ensure completeness of the total trial wave function and to compensate for orthogonality constraints imposed on the continuum orbitals.

The use of nonorthogonal one-electron radial functions in the BSR method, on the other hand, allows us to avoid these configurations for compensating orthogonality restrictions. Hence, the bound channels in the present model were only used to describe the true bound states of the e-Si collision system, namely, the $3s^2\,3p^3\,^4S$, ^2D, and ^2P states of the Si^- ion. We employed extensive MCHF expansions for these states to ensure their energies to be close to the experimental values of -1.389, -0.527, and -0.029 eV, respectively [22]. Since the χ_i functions are already constructed in multiconfiguration form, the b_{ik} coefficients in our implementation represent the entire $(N+1)$-electron bound-state expansion. This procedure has practical advantages in avoiding a pseudoresonance structure in the scattering solutions.

The R-matrix radius was set to $60a_0$, where $a_0 = 0.529 \times 10^{-10}$ m is the Bohr radius. This value is sufficiently large for all target orbitals to be effectively zero at the boundary. We employed 140 B-splines to span this radial range. Such a relatively large number of splines makes it possible to cover electron energies up to 150 eV. We calculated partial waves for total orbital angular momenta $L \leqslant 20$ numerically and then used a top-up procedure to estimate the contribution to the cross sections from even higher L values. The calculation for the external region was performed using the flexible asymptotic R-matrix (FARM) package [23].

III. RESULTS

Cross sections as a function of energy for the most important transitions from the ground state and the metastable states are presented in Figs. 1–4. All electron energies are given relative to the $3s^2\,3p^2\,^3P$ ground state. Due to the almost complete absence of other theoretical results and experimental data, we sometimes compare predictions from two sets of calculations, carried out with and without including the polarized pseudostates. This allows us to check, at least to some extent, the sensitivity of the results on the details of the model.

The elastic and momentum transfer cross sections for electron scattering from the three states with the ground-state configuration $3s^2\,3p^2$are presented in Fig. 1. All cross sections exhibit a similar energy dependence with a sharp maximum at 4.2 eV, which is caused by the strong $3s3p^4\,^4P$ resonance. The narrow maximum at the elastic threshold also originates from the ^4P partial wave in the ks scattering channel, thus indicating a large scattering length. There are other resonance features, but their contributions are negligible. Figure 1 only shows

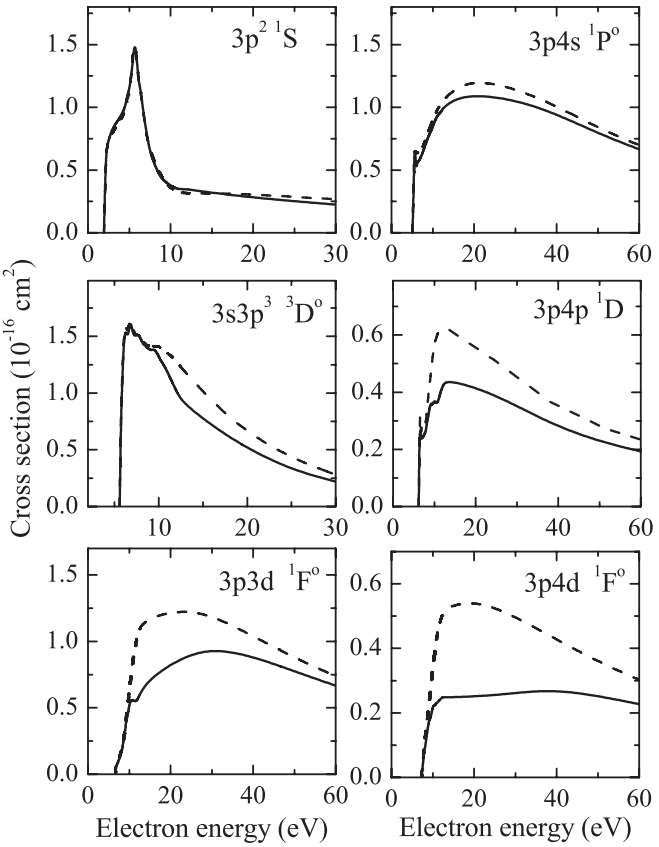

FIG. 3. Cross sections as a function of collision energy for the most important transitions from the $3s^2\,3p^2\,{}^1D$ metastable state (solid lines), compared to results from calculations without pseudostates (dashed lines).

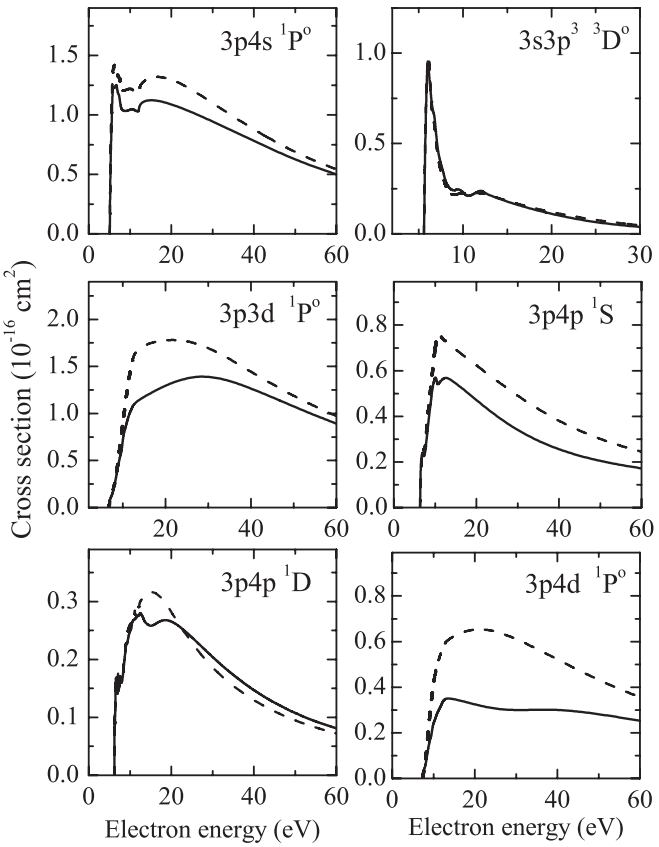

FIG. 4. Cross sections as a function of collision energy for the most important transitions from the $3s^2\,3p^2\,{}^1S$ metastable state (solid lines), compared to results from calculations without pseudostates (dashed lines).

results from calculations with polarized pseudostates. The 34-state BSR scattering model yields very similar results, except in the near-threshold region below 0.01 eV, where inclusion of the pseudostates reduces the near-threshold maximum.

The excitation cross sections for some important transitions from the $3s^2\,3p^2\,{}^3P$ ground state are presented in Fig. 2. The spin-forbidden transitions to the ^1D and ^1S states of the same configuration show the typical character of exchange transitions: The cross sections exhibit a dominant maximum at low energies and quickly decrease at higher energies. The pseudostates only have a small influence on the spin-forbidden transitions. While this finding appears somewhat surprising, tests showed that the reason is the dominance of resonance contributions in particular partial waves.

As seen in the panels for transitions to the $3s^2\,3p4s^3P^o$, $3s^2\,3p3d^3D^o$, and $3s^2\,3p4p^3P$ states, however, the polarized pseudostates have a considerable effect on the spin-allowed transitions over a wide range of incident electron energies. Tests showed that the sensitivity of the results to the inclusion of these states is spread out over several partial-wave symmetries. Since the polarized pseudostates describe in part the excitation to the target continuum, we conclude that the close-coupling expansion converges slowly for the higher-lying states.

The only previous results available for comparison are distorted-wave (DW) calculations by Pindzola *et al.* [4] for the $3s^2\,3p\,{}^3P \rightarrow {}^1S$ transition within the ground-state configuration of neutral silicon. These authors used the Hartree-Fock (HF) and adiabatic-exchange (AE) approximations, where the latter includes the adiabatic polarization potential for the scattering electron. They found that exchange and polarization effects are extremely important for the ${}^3P \rightarrow {}^1S$ excitation process and that nonorthogonality effects between scattering and bound orbitals of the same symmetry play a crucial role. A comparison with these DW calculations is also shown in Fig. 2. The significant deviations of the DW results from the present calculations is likely due to the accuracy of the target wave functions as well as the channel-coupling effects included in our model. The AE approximation predicts a similar energy dependence but considerable differences in the magnitude of the cross sections. Nevertheless, we confirm the conclusion of Pindzola *et al.* that their predictions should be accurate within a factor of about 2.

The results for excitation from the $3s^2\,3p^2\,{}^1D$ and $3s^2\,3p^2\,{}^1S$ metastable states, presented in Figs. 3 and 4, exhibit a similar energy dependence. Including the pseudostates once again leads to significant changes in the results for spin-allowed transitions, and these corrections are considerable for the weak transitions. On the other hand, the excitation of the $3s^2\,3p^2\,{}^1D \rightarrow 3s^2\,3p^2\,{}^1S$ forbidden transition is almost unaffected by the pseudostates. This is due to the dominant contribution from the $3s3p^4\,{}^2D$ resonance, which causes the

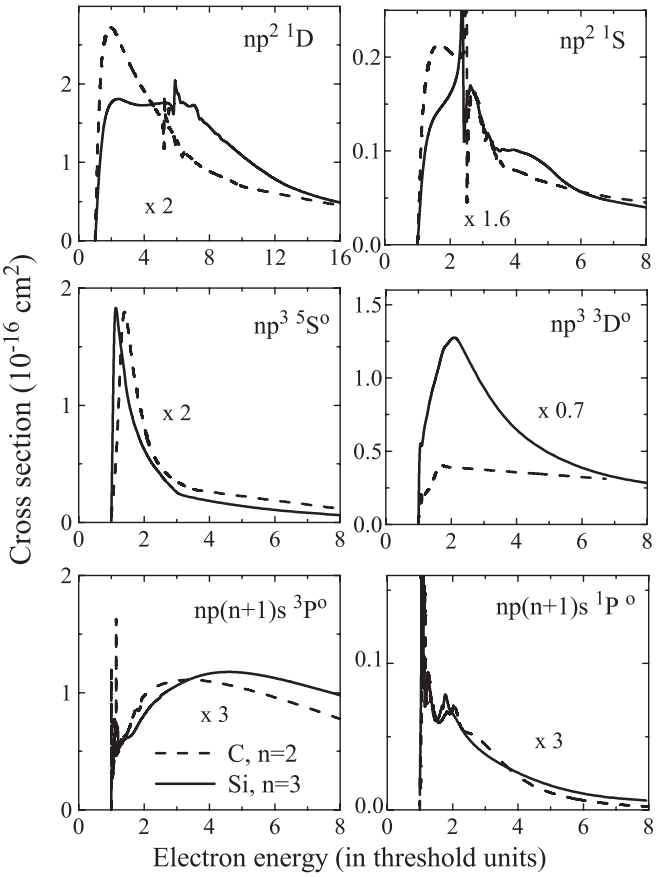

FIG. 5. Comparison of predictions for electron-impact excitation of silicon and carbon from their respective ground states. The solid lines represent the 34-state BSR calculations for *e*-Si and the dashed lines the 29-state BSR calculations for *e*-C [10]. The actual cross sections for C were multiplied by the scale factors shown in the legend.

cross section for this transition to exhibit a strong maximum at 5.6 eV. The same resonance also leads to strong near-threshold maxima in the excitation of the $3s3p^3\,{}^3D^o$ state.

Finally, it is interesting to compare the present results for *e*-Si collisions with the corresponding electron-impact cross sections in carbon. While carbon is in the same group of the periodic table as silicon, correlation effects differ significantly in the two elements. In silicon, the $3d$ orbital is localized in the same radial regime as the $3s$ and $3p$ orbitals that define the ground-state configuration. Consequently, an accurate determination of the target wave functions, particularly in the neutral atom, is much more difficult in silicon than it is in carbon where the $3d$ orbital is concentrated much farther outside.

Figure 5 compares the cross sections for excitation of the lowest six levels in C and Si from the ground state. The electron energies are given in units of the threshold energy to allow for a direct comparison. Also shown is a scaling factor for the *e*-C cross sections. Except for excitation of the $3s3p^3\,{}^3D$ state, we note a strong similarity in the energy dependence of the corresponding cross sections in C and Si, with the *e*-Si cross sections generally (again except for the ${}^3D^o$ state) having a significantly larger magnitude.

IV. SUMMARY

We have presented theoretical cross sections for elastic scattering and electron-impact excitation of Si from its ground state and metastable excited states. The calculations were performed with the BSR code, in which a *B*-spline basis is employed to represent the continuum functions inside the *R*-matrix sphere. Another distinguishing feature of the BSR calculations is the use of nonorthogonal orbitals, both in constructing the target wave functions and in representing the scattering functions. This technique allows us to optimize the atomic wave function for each state independently, and hence to generate an accurate target description.

Given the lack of available experimental data, it is crucial that the theoretical predictions be validated in some way. To this effect, we used two scattering models to check such important effects as target polarization and excitation to the target continuum, i.e., ionization. The cross sections for elastic scattering as well as for transitions between the ground state and the metastable states are very similar in the two scattering models, a finding that provides some confidence in the accuracy of these numbers. For some transitions to higher-lying states, however, significant differences between the results from the two calculations indicate a slow convergence of the close-coupling expansion in these cases. Unfortunately, performing even larger calculations goes beyond our currently available computational resources.

Given the importance of silicon in various applications, it seems highly desirable to have independent experimental data as well as results from other calculations in order to establish a reliable database of these cross sections. Electronic files with the current results, for electron energies up to 100 eV, are available from the authors upon request.

ACKNOWLEDGMENTS

This work was supported by the United States National Science Foundation under grants PHY-0903818 (OZ and KB), PHY-1068140 (KB), and the TeraGrid/XSEDE allocation TG-PHY090031. Additional support from Drake University through a Troyer Research Fellowship (KB) is also gratefully acknowledged.

[1] P. M. Mendes, S. Jacke, K. Critchley, J. Plaza, Yu Chen, K. Nikitin, R. E. Palmer, J. A. Preece, S. D. Evans, and D. Fitzmaurice, Langmuir **20**, 3766 (2004).

[2] J. Biskupek, U. Kaiser, and F. Falk, J. Electron Microsc. **57**, 83 (2008).

[3] I. Torchinsky, N. Amdursky, A. Inberg, and G. Rosenman, Appl. Phys. Lett. **96**, 093106 (2010).

[4] M. S. Pindzola, A. K. Bhatia, and A. Temkin, Phys. Rev. A **15**, 35 (1977).

[5] O. Zatsarinny, Comput. Phys. Commun. **174**, 273 (2006).

[6] O. Zatsarinny and K. Bartschat, Phys. Rev. A **77**, 062701 (2008).
[7] O. Zatsarinny and K. Bartschat, AIP Conf. Proc. **1344**, 125 (2011).
[8] O. Zatsarinny and S. S. Tayal, J. Phys. B **35**, 241 (2002).
[9] O. Zatsarinny and S. S. Tayal, J. Phys. B **34**, 3383 (2001).
[10] O. Zatsarinny, K. Bartschat, L. Bandurina, and V. Gedeon, Phys. Rev. A **71**, 042702 (2005).
[11] C. F. Fischer, Phys. Rev. A **71**, 042506 (2005).
[12] O. Zatsarinny and C. Froese Fischer, J. Phys. B **35**, 4669 (2002).
[13] C. Froese Fischer, Comput. Phys. Commun. **176**, 559 (2007).
[14] [http://physics.nist.gov/cgi-bin/AtData].
[15] T. R. O'Brian and J. E. Lawler, Phys. Rev. A **44**, 7134 (1991).
[16] P. G. Burke and J. F. B. Mitchell, J. Phys. B **7**, 665 (1974).
[17] O. Zatsarinny, K. Bartschat, and M. Allan, Phys. Rev. A **83**, 032713 (2011).
[18] G. Maroulis and C. Pouchan, J. Phys. B **36**, 2011 (2003).
[19] C. Lupinetti and A. J. Thakkar, J. Chem. Phys. **122**, 044301 (2005).
[20] C. Thierfelder, B. Assadollahzadeh, P. Schwerdtfeger, S. Schäfer, and R. Schäfer, Phys. Rev. A **78**, 052506 (2008).
[21] P. G. Burke, *R-Matrix Theory of Atomic Collisions* (Springer-Verlag, Berlin, 2011).
[22] M. Scheer, R. C. Bilodeau, C. A. Brodie, and H. K. Haugen, Phys. Rev. A **58**, 2844 (1998).
[23] V. M. Burke and C. J. Noble, Comput. Phys. Commun. **85**, 471 (1995).